

Optically induced orientational transitions in nematics with planar alignment

Dmitry O. Krimer*

Max Planck Institute for the Physics of Complex Systems,
Nöthnitzer Str. 38, D-01187 Dresden, Germany

(Dated: November 13, 2018)

Theoretical study of dynamical phenomena induced by a linearly polarized plane wave incident perpendicularly on a planar aligned nematic layer with the light intensity as the control parameter is reported. We find the threshold of the Optically Induced Fréedericksz Transition for the planar state as a function of the problem parameters. It occurs that the threshold is substantially lower than that expected before. Above the primary instability the director settles either to a stationary or to an oscillatory states depending on a thickness of the layer. These states become unstable at a secondary threshold through a heteroclinic bifurcation and the director settles to a new stationary distorted state.

PACS numbers: 42.70.Df, 05.45.-a, 42.65.Sf

Optical phenomena exhibited by nematic liquid crystals has been a subject of intensive study during the last few decades. A nematic behaves optically as a uniaxial anisotropic medium with the optical axis along the local molecular orientation described by the director $\mathbf{n}(\mathbf{r}, t)$. The dielectric tensor governing the propagation of light is anisotropic and depends on \mathbf{n} . There are two competing mechanisms which determine the nematic alignment. On one hand, it is enforced by the anchoring forces at the confining surfaces. On the other hand the electric field of the incident light exerts a torque which may conflict with the boundary-imposed alignment. The torque increases with an increase in the light intensity. Eventually, at a certain light intensity the boundary-imposed alignment becomes unstable being replaced by the light-imposed one (Optically Induced Fréedericksz Transition) which in turn affects the light propagation [1]. A large variety of nonlinear phenomena occurs as a result this feedback [2]. The possibility of dynamical changes of the nematic refractive index employing the orientational phenomena, has attracted recently much attention in the context of construction of all-optical devices based on photonic structures infiltrated with liquid crystals, see e.g. [3] and references therein. The goal of this paper is elaborated theoretical study of light induced phenomena in a nematic cell with planar alignment (without photonic structure) which is much less explored than that with the homeotropic one. This problem was considered before in [4] where a linear analysis of the planar state with respect to a restricted class of perturbations was done. In the present paper we perform the general linear analysis with respect to arbitrary (small) perturbations. We show that the planar state might lose stability either through a stationary bifurcation or through a Hopf bifurcation when the thickness of the layer is above a certain critical value. The thresholds for the primary instability are substantially lower than those predicted before.

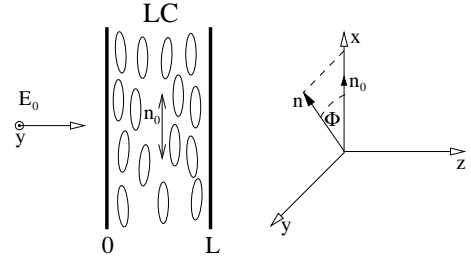


FIG. 1: Geometry of the setup: linearly polarized light along the y direction incident perpendicularly on a nematic layer with the director $\mathbf{n}_0 \parallel \mathbf{x}$ (planar state). The components of the director \mathbf{n} are described in terms of the twist angle Φ ($\Phi = 0$ in the planar state).

Above the Hopf bifurcation the system settles to an oscillatory state. This state, in turn, becomes unstable at some higher value of intensity where the transition to a new stationary distorted state via a heteroclinic bifurcation occurs.

We consider a linearly polarized along the y direction plane wave, propagating along the z axis. The wave incidents perpendicularly to a nematic layer, see Fig. 1. Initially the director is orientated along the x axis (planar alignment) and keeps its orientation at the boundaries (rigid boundary conditions). We restrict the consideration analyzing only spatially-homogeneous in the layer plane solutions which depend on the z coordinate solely. To describe the director orientation the twist angle $\Phi(z, t)$ is introduced, so that $\mathbf{n} = (\cos \Phi, \sin \Phi, 0)$. The starting point is the set of nematodynamic equations coupled with Maxwell's equations for the propagation of light [5]. The dynamical equation of motion for $\Phi(z, t)$ is obtained from the balance of torques (elastic, electromagnetic and viscous) acting on the nematic. The components of the electric field might be represented in terms of the amplitudes of the ordinary and extraordinary waves A_e, A_o that vary slowly with z on the scale $(k_0 L)^{-1}$ (see e.g. [6]), where $k_0 = \omega/c$ is the wavenumber of the incident wave and L stands for the layer thickness. Finally, in the absence of a velocity field the coupled PDE for Φ and ordinary differential equations (ODEs) for A_e

*Electronic address: krimer@pks.mpg.de

and A_o can be written as follows [6]

$$\partial_t \Phi = \partial_z^2 \Phi + 2\rho \tilde{k}_0^2 \text{Re} \left[A_e A_o^* e^{i\tilde{k}_0 z} \right] \quad (1)$$

$$\partial_z A_o = -(\partial_z \Phi) e^{i\tilde{k}_0 z} A_e, \quad \partial_z A_e = (\partial_z \Phi) e^{-i\tilde{k}_0 z} A_o, \quad (2)$$

where \tilde{k}_0 is dimensionless thickness $\tilde{k}_0 = 2L\delta n/\lambda$ with $\delta n = n_e - n_o$ (n_e and n_o are, the refractive indices of the ordinary and extraordinary light, respectively) and λ is the incident light wavelength. To make the variables in Eqs. (1), (2) dimensionless they have undergone the following scale transformation: $t \rightarrow t/\tau$; $z \rightarrow \pi z/L$; amplitudes $A_{e,o}$ have been normalized over the electric field amplitude of the incident light; $\rho = I/I_c$, where I stands for the incident light intensity. Here $\tau = \gamma_1 L^2/\pi^2 K_2$ is characteristic relaxation time of the director motion and $I_c = 8\pi^2 c K_2 n_e \delta n/\lambda^2 (n_e + n_o)$, K_2 is the twist elastic constant and $\gamma_1 = \alpha_3 - \alpha_2$ is the rotational viscosity.

The boundary condition for Φ and initial conditions for A_o , A_e at $z = 0$ read as follows:

$$\Phi_{z=0,\pi}(t) = 0, \quad |A_{o0}|^2 = 1, \quad |A_{e0}|^2 = 0, \quad A_{e0} A_{o0}^* = 0. \quad (3)$$

Note that owing to the reflection symmetry with respect to the y direction Eqs. (1-3) are invariant under the transformation $S: \{\Phi, A_e, A_o\} \rightarrow \{-\Phi, \mp A_e, \pm A_o\}$. It is convenient to represent the solution of Eqs. (1)-(3) as a series $\Phi(z, t) = \sum_n \Phi_n(t) \sin(nz)$, where each term of the sum satisfies the boundary conditions Eq. (3) identically. Then, Eqs. (1)-(3) are transformed into an infinite set of coupled equations for Φ_n . To make the problem tractable the set is truncated at a certain large enough number of equations N which are solved numerically by the standard Runge-Kutta method. The error caused by the truncation is controlled by test runs with double and triple number of the modes. For every set of parameters N is selected so that the difference between the routine and test runs is better than 1%. Regarding equations for A_o , A_e , they have to be solved dynamically at each step of numerical integration for time t . In addition, we perform a linear analysis (numerically) of the stationary distorted states ($\partial_t \Phi_n = 0$) by calculating the corresponding Jacobians.

The starting point of the study is the linear stability analysis of the planar state ($\Phi(z, t) = 0$). The linearized integro-differential equation for $\Phi(z, t) = \Phi(z) \exp(\sigma t)$ is as follows:

$$\partial_z^2 \Phi + 2\rho \tilde{k}_0^2 \left(\Phi + \tilde{k}_0 \int_0^z \Phi(z') \sin[\tilde{k}_0(z' - z)] dz' \right) = \sigma \Phi. \quad (4)$$

It results in the following set of equations for Φ_n (eigenvalue problem):

$$\sum_n A_{mn} \Phi_n = \sigma \Phi_m \quad (5)$$

$$A_{mn} = \left(\frac{2\rho \tilde{k}_0^2}{n^2 - \tilde{k}_0^2} - 1 \right) n^2 \delta_{mn} + \frac{4(-1)^m \rho \tilde{k}_0^3 mn \sin(\pi \tilde{k}_0)}{\pi(m^2 - \tilde{k}_0^2)(n^2 - \tilde{k}_0^2)}.$$

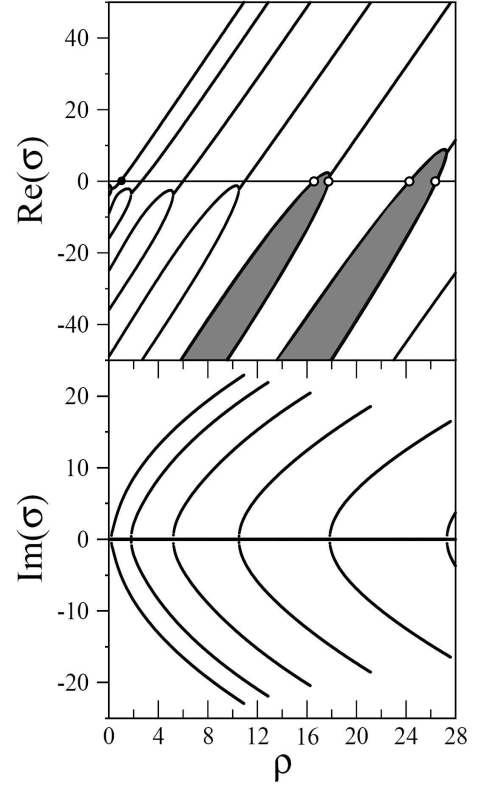


FIG. 2: $\text{Re}(\sigma)$ and $\text{Im}(\sigma)$ vs. ρ for $\tilde{k}_0 = 1.6$. Filled circle: primary threshold ($\rho_1 = 0.95$, Hopf bifurcation). Shaded tongues cross abscissa at, respectively, $\rho_1^* = 16.6$, $\rho_2^* = 17.8$, $\rho_3^* = 24.3$ and $\rho_4^* = 26.5$ depicted by empty circles.

The solvability condition for Eq. (5) requires $\det(A - \sigma I) = 0$. It brings about infinite number of eigenvalues σ_n . However, at $n \gg \tilde{k}_0^2$ or (and) $m \gg \tilde{k}_0^2$ the off diagonal elements of matrix A_{mn} decay as $1/n$ or (and) $1/m$, while the diagonal elements equal $-n^2$. Then, in the leading approximation $\det(A - \sigma I)$ factorizes for a product of infinite number of the diagonal elements at $n > N$ (which give stable real eigenvalues $\sigma_n \approx -n^2$ related to elastic relaxation) and a minor $N \times N$, where $N \gg \tilde{k}_0^2$. Eigenvalues of the minor are related to light-induced perturbations and should be inspected more carefully. These arguments provides us with the natural truncation scale $\sim \tilde{k}_0^2$. Note that the minimal number of modes for adequate description of the phenomenon increases as L^2 . The planar state loses stability when the real part of (at least) one of the eigenvalues $\text{Re}(\sigma_n)$ becomes positive. It should be stressed that matrix A_{mn} is not Hermitian and may have complex eigenvalues, in other words unstable modes may be oscillatory.

Typical results of the discussed stability analysis are presented on Fig. 2, where $\text{Re}(\sigma_n)$ and $\text{Im}(\sigma_n)$ versus ρ are shown for $\tilde{k}_0 = 1.6$. (The calculation are made for $N = 20$.) It is seen that $\text{Re}(\sigma_n)$ forms a tongued structure with a family of branches which, at first, appear as pairs of purely real branches that go almost parallel to each other as ρ increases, but then the pair merges at a certain $\rho \geq \rho_{top}^{(n)}$. Next, the branches continue as a pair

of complex conjugate modes. Some of the purely real branches cross the zero line at intensities ρ given by the formula

$$\frac{2\rho \cdot \sin[\pi \tilde{k}_0 \sqrt{1+2\rho}]}{\pi \tilde{k}_0 \sqrt{1+2\rho}} = -1, \quad (6)$$

which was derived in [4]. The first two tongues depicted by shaded areas cross the abscissa at $\rho_1^* = 16.6$, $\rho_2^* = 17.8$, $\rho_3^* = 24.3$ and $\rho_4^* = 26.5$, respectively, and are the same as ones shown in Fig. 1 of [4]. (The dimensionless $\tilde{L} = 5$ introduced there corresponds to $\tilde{k}_0 = \tilde{L}/\pi \sim 1.6$ used in our calculations.) In [4] such a structure was interpreted as a series of alternate stable and unstable intervals for the planar state as the light intensity increases with the lowest threshold for instability given by $\rho_1^* = 16.6$. However, in reality, the planar state loses stability via a Hopf bifurcation at much lower value $\rho_1 = 0.95$ (filled circle on Fig. 2) and *never* restores stability at higher intensities again. In fact, the reason for such a difference with the results of [4] is that for solving the eigenvalue problem (5) therein a particular (not a general) form of a trial solution was used [see [4], Eqs. (6,10)]. As a result, the growth rates turned out to be *a priori* real instead of being complex and, thus, the ones with $\text{Im}(\sigma) \neq 0$ predicted here have been not caught. The stability diagram in the (\tilde{k}_0, ρ) plane is shown in Fig. 3 by solid lines and the thresholds calculated using the Eq. (6) are depicted by dashed lines. It is interesting, that below a certain critical value $\tilde{k}_0^{(c)} < 0.64$ (corresponding to $\tilde{L} = 2$ in [4]), the primary bifurcation is stationary indeed and the values of thresholds are correctly described by Eq. (6). In that case, the very first tongue crosses the ρ axis (in contrast to the situation for $\tilde{k}_0 = 1.6 > \tilde{k}_0^{(c)}$ depicted in Fig. 2 where the first tongue is under the abscissa) and at the threshold the largest growth rate corresponds to the purely real branch. When approaching $\tilde{k}_0^{(c)}$ from below, this first tongue goes down and, finally, at $\tilde{k}_0 = \tilde{k}_0^{(c)}$ the whole tongue lies under the ρ axis. Note, that transition to another branch with $\text{Im}[\sigma] \neq 0$ is accompanied by a stepwise change of the threshold intensity. Such a behavior is related to the inclined structure of the tongues (see Fig. 3). It should be stressed that for $\tilde{k}_0 > \tilde{k}_0^{(c)}$, the true values of the thresholds differs from the ones predicted by Eq. (6) in one order, and with increase of \tilde{k}_0 quite rapidly, in two orders of magnitude. The true threshold of the primary instability, decreases with an increase in \tilde{k}_0 from $I = 3.3 I_c$ at $\tilde{k}_0 = \tilde{k}_0^{(c)}$ to $0.5 I_c$ at $\tilde{k}_0 = 8$ and then practically does not change at further increase in the \tilde{k}_0 , see Fig. 3. To obtain a stability diagram in the dimensional (L, I) plane one should rescale \tilde{k}_0 and ρ -axes of Fig. 3 multiplying them by $\lambda/(2\delta n)$ and I_c , respectively. In experiment one should take nematics with rather small values of δn to avoid very large values for thresholds which are of the order of I_c . For instance, for $\delta n = 5 \cdot 10^{-3}$, $K_2 = 2.5 \cdot 10^{-7} \text{ dyn}$ and $\lambda = 532 \text{ nm}$ the value of I_c is 52 kW/cm^2 and the critical

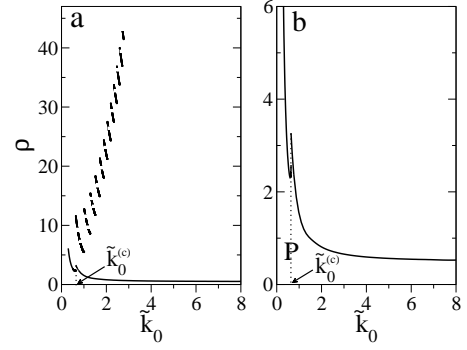


FIG. 3: Solid lines: stability diagram of the planar state on the (\tilde{k}_0, ρ) plane. Dashed lines on (a): thresholds calculated using the Eq. (6). Solid line with $\tilde{k}_0 < \tilde{k}_0^{(c)}$ ($\tilde{k}_0 \geq \tilde{k}_0^{(c)}$) corresponds to stationary (Hopf) bifurcation. P: region of stability of the planar state

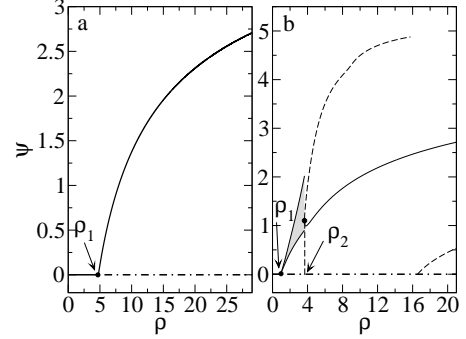


FIG. 4: Bifurcation diagrams for (a) $\tilde{k}_0 = 0.5$ and (b) $\tilde{k}_0 = 1.6$: parameter of reorientation Ψ vs. ρ . Solid (dashed) curves correspond to stable (unstable) stationary solutions. ρ_1 : primary instability of the planar state. (a) $\rho_1 = 4.76$ (stationary bifurcation); (b) $\rho_1 = 0.95$ (Hopf bifurcation). Gray region (confined by two lines): oscillatory states of the director. $\rho_2 = 3.65$: secondary instability (heteroclinic bifurcation).

length $L^{(c)} = \tilde{k}_0^{(c)} \lambda / (2\delta n)$ is $34 \mu\text{m}$.

It is worth noting, that the linear integro-differential equation (5) appears in the framework of linear analysis of another problem, namely the one with a linearly polarized ordinary light wave incident at a small oblique angle on a thin layer of homeotropically oriented nematic [7, 8]. The only difference is that there one deals with the normalized incidence angle κ instead of \tilde{k}_0 used here. It is well known that stability diagram in the (ρ, κ) plane might be calculated with good accuracy in the framework of a two modes approximation (for $\kappa < 1$) and consists of a line of stationary instability which joins the line of Hopf instability in the Takens-Bogdanov point [8]. The line of stationary instability exists only below a certain critical value of $\kappa^{(c)}$ and as we checked out is indeed described by the formula (6) after rewriting it in corresponding quantities. However, above $\kappa^{(c)}$ the homeotropic state loses stability always via a Hopf bifurcation and the formula (6) is not applicable anymore. Moreover, the homeotropic state will never be alternatively stable and

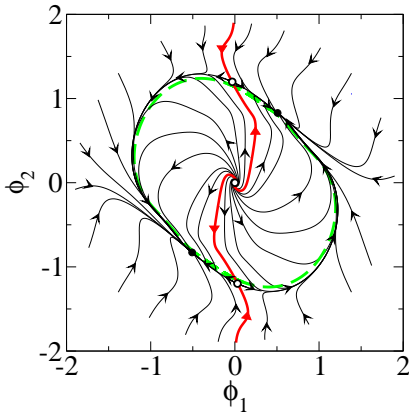


FIG. 5: Dynamics near the secondary threshold $\rho_2 = 3.6530$: director trajectories at $\rho = 3.7967 > \rho_2$ in the plane of first two modes (Φ_1, Φ_2) . Starting from different initial condition the system settles to one of the two stable nodes (filled circles). Red curve: separatrix. Empty circles: unstable fixed points (saddles). Origin: unstable spatially uniform planar state (focus). Dashed green line: limit cycle at $\rho = 3.638 < \rho_2$.

unstable for any κ and at higher intensities a very complex dynamics occurs [2]. Here we have a similar picture but with respect to the critical $\tilde{k}_0^{(c)}$.

We choose a sum of squares of all modes $\Psi = \sum_n \Phi_n^2$ as a theoretical measure of reorientation inside nematic. It is an appropriate quantity because $\Psi = 0$ for the planar state, it increases with increasing of the reorientation, saturates to a certain value since the amplitudes damp after certain n and is independent on material parameters. In Fig. 4 typical bifurcation diagrams are shown for $\tilde{k}_0 < \tilde{k}_0^{(c)}$ and $\tilde{k}_0 > \tilde{k}_0^{(c)}$. The planar state remains stable when $\rho < \rho_1$. At $\rho = \rho_1$ we deal with a continuous transition via either a stationary for $\tilde{k}_0 < \tilde{k}_0^{(c)}$ or a Hopf bifurcation in opposite case. Above the threshold and for $\tilde{k}_0 < \tilde{k}_0^{(c)}$ the director settles to a stationary distorted state, whereas for $\tilde{k}_0 > \tilde{k}_0^{(c)}$ to an oscillatory one. In latter regime, the lower and the upper lines depicted in Fig. 4(b) bound the region in gray and correspond to the minimum and maximum values taken by Ψ during its oscillation. The director motions develops along the limit cycle in the space of Φ_n (which is infinite). Importantly, the planar state is always unstable for $\rho > \rho_1$ in both cases. In some narrow region around $\rho_2 = 3.65$ the period of oscillations increases progressively with increasing light intensity, and oscillations become substantially anharmonic. The period diverges at $\rho = \rho_2$ which cor-

respond to a secondary bifurcation transforming the system into a new stationary distorted state. The dynamics near the threshold is summarized in the projection of the true phase trajectory on the plane (Φ_1, Φ_2) , see Fig. 5. The bifurcation at $\rho = \rho_2$ belongs to rather a rare type and corresponds to the following. Above ρ_2 a system has two pairs of stationary nontrivial solutions which are mutual images under the symmetry transformation S . The first pair is represented by a stable node and its image and the second one by a saddle and its image. There is also a trivial solution which is represented by an unstable focus corresponding to the spatially uniform planar state. Starting from different initial conditions the system eventually settles to one of the stable nodes. A separatrix, which partitions phase plane onto the basins of attraction for the two stable nodes, goes through the two saddles and the unstable focus. Approaching ρ_2 from above, the saddle and node go closer and closer to each other and finally merge at $\rho = \rho_2$. At this point the limit cycle appears which exist for $\rho_1 < \rho < \rho_2$. It is worth noting that the symmetry S is spontaneously broken at the secondary bifurcation. We checked that the bifurcation scenario displayed in Fig. 4 exists over wide region of \tilde{k}_0 . However, the oscillatory regime seems to be more complex for $\tilde{k}_0 \geq 3$ than that described above.

In conclusion, we have studied theoretically the transitions induced by linearly polarized light incident perpendicularly to a layer of nematic that has initially spatially uniform planar alignment. We have found the primary threshold as a function of (normalized) thickness of the layer by performing a linear analysis of the basic state. Our numerical analysis of the problem shows that, with increasing light intensity, the planar state becomes unstable in a favor of either a stationary distorted state when the thickness is below a certain critical value, or to an oscillatory state if the thickness is above the critical value. As the intensity increases further, the oscillatory state disappears via a secondary bifurcation. At the bifurcation point two identical saddle-node fixed points are born on opposite sites of the limit cycle. It results in divergence of the period of oscillations and partition of the limit cycle into two heteroclinic orbits. Further increase in the intensity brings about splitting each of the fixed point into a stable node and a saddle. In typical cases the calculated thresholds have values substantially lower than those believed before.

The author wishes to thank M.I. Tribelsky, S. Flach, A. Miroshnichenko, E. Brasselet and A. Krekhov for helpful discussions and comments.

- [1] N. V. Tabiryan, A. V. Sukhov, and B. Y. Zel'dovich, *Mol. Cryst. Liq. Cryst.* **136**, 1 (1986).
- [2] G. Demeter and D.O. Krimer, *Phys. Reports*, **448**, 133 (2007)
- [3] A. E. Miroshnichenko, E. Brasselet, Y. S. Kivshar, *Appl. Phys. Lett.* **92** 53306 (2008); U. A. Laudyn, A. E. Miroshnichenko, W. Krolikowski, D. F. Chen, Y. S. Kivshar, M. A. Karpierz, *Appl. Phys. Lett.* **92** 203304 (2008)
- [4] E. Santamato, G. Abbater, P. Maddalena and Y.R. Shen,

- Phys. Rev. A* **36**, 2389 (1987).
- [5] P. G. de Gennes and J. Prost, *The physics of liquid crystals* (Clarendon press, Oxford, 1993).
- [6] D. O. Krimer, PhD Thesis, University of Bayreuth (2004); URL: <http://opus.ub.uni-bayreuth.de/volltexte/2004/98/>; E. Brasselet, T.V. Galstian, L. J. Dube, D. O. Krimer and L.

- Kramer, J. Opt. Soc. Am. B, **22**, 1671 (2005).
- [7] N.V. Tabiryan, A.L. Tabiryan-Murazyan, V. Carbone, G. Cipparrone, C. Umeton, C. Versace, T. Tschudi, Optics Comm. **154**, 70 (1998).
- [8] G. Demeter, Phys. Rev. E **61**, 6678 (2000); D. O. Krimer, G. Demeter and L. Kramer, Phys. Rev. E **66**, 031707 (2002).